

The peculiar response of Kelvin-Voigt chains with a free end

Rupayan Saha^{1,*} and Matthias Krüger^{1,†}

¹*Institut für Theoretische Physik, Georg-August Universität Göttingen, 37077 Göttingen, Germany*
(Dated: May 26, 2026)

We exactly solve a model of a heterogeneous chain of overdamped, harmonically coupled particles with momentum-conserving dissipation. Despite being governed by a non-symmetric drift operator, the system admits an analytical diagonalization by use of a forward-difference transformation. In case of one free end, the response matrix shows a peculiar staircase form: the response of particle i to a force acting on particle j is independent of the properties and the length of the chain-part between i and j . For rank-deficient interaction matrices, the state space is decomposed into free and constrained subspaces. We demonstrate that this separation has clear physical consequences: the free subspace governs steady state responses, while the constraint subspace governs the relaxation after cessation of forcing. These results establish a framework for analyzing heterogeneous overdamped dynamics with momentum conservation.

I. INTRODUCTION

The one-dimensional harmonic chain is a paradigmatic model for collective dynamics in many-body systems, combining analytical tractability with broad physical relevance. Its legacy spans from Huygens' foundational works on synchronized pendulums [1] and the study of small oscillations in the eighteenth century [2] to the early twentieth-century development of lattice dynamics and phonon theory in solids [3–6]. In the latter half of the twentieth century, the growing interest in soft matter and polymer physics led to the modification of the same framework into the overdamped limit [7], eliminating inertia in favor of dissipation with respect to a surrounding “bath” [8], acting as a *local* momentum sink. In this standard case with homogeneous interaction (stiffness) and dissipation (friction), the normal modes coincide with those of the inertial harmonic chain [9] with oscillation frequencies replaced by relaxation rates.

However, allowing for spatial heterogeneity in elastic or dissipative properties, as, e.g., encountered in chemically heterogeneous polymers, coarse-grained biomolecular models, or spatially heterogeneous hydrodynamic environments, often precludes a normal mode decomposition, and hence motivates numerical approaches [10, 11], with few analytical exceptions [12]. Furthermore, incorporating *internal* friction, reflecting dissipation within the polymer or mediated by the solvent [13–15], further anticipate the emergence of relative and momentum-conserving dissipation, characteristic of hydrodynamic descriptions [16]. A qualitatively new regime emerges when momentum conservation is enforced by modeling dissipation as arising *solely* from internal friction within the surrounding medium, rather than from coupling to a fixed background. Such momentum-conserving dissipation, naturally realized in dissipative particle dynamics (DPD) [17, 18], and related approaches [19–22], gives rise to relative friction, whereby the dissipative force on a degree of freedom depends on its relative motion with respect to neighboring degrees of freedom.

Remarkably, although spatial heterogeneity in general impedes analytical treatment, momentum-conserving dissipation with nearest-neighbor structure keeps the system exactly solvable [23–25]. We show here that this is achieved by introducing a forward-difference transformation that maps the dynamics from site variables (physical displacements) to bond variables (relative displacements). In the present setup, both the stiffness (K) and dissipation (Γ) matrices acquire a compatible structure that can be expressed in terms of difference operators, leading to an exact decoupling of the dynamics. Consequently, the drift matrix, $W = \Gamma^{-1}K$, remains diagonalizable even in the presence of heterogeneity. Thus, the same physical ingredients that introduce complexity – spatial variation and hydrodynamic consistency – also impose sufficient structure to restore analytical tractability.

The same structure manifests in strikingly nonlocal mechanical responses. In particular, we demonstrate that chains with an open end exhibit particularly counter-intuitive responses: the response of particle i to a force acting on particle j does not depend on the properties or length of the chain in between i and j , encoded in a staircase pattern in the response matrix. We refer to this as an “X-ray vision” property, where the response effectively sees through intermediate heterogeneity.

While the staircase response already reveals the peculiar signal propagation, a deeper physical distinction emerges when we apply this framework to viscoelastic fluids which requires an underconstrained, rank-deficient interaction matrix K , possessing free modes associated with irreversible rearrangements (reminiscent of a fluid), while retaining

* rupayan.saha@uni-goettingen.de

† matthias.kruger@uni-goettingen.de

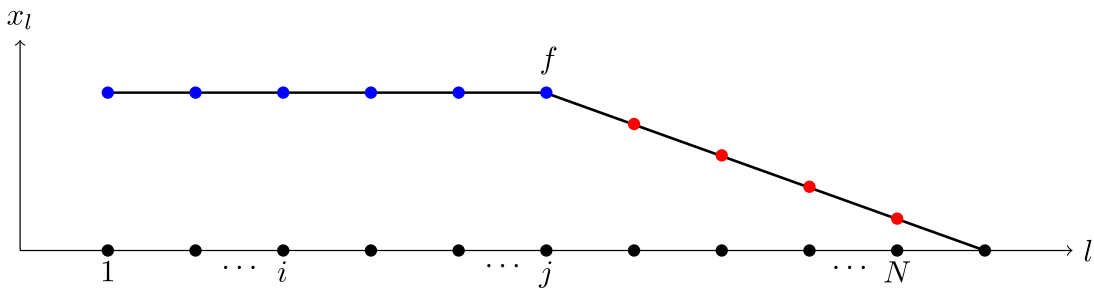


FIG. 1. **Displacement profile in a massless undamped harmonic chain** of length N , with left end free and the right end (site $N + 1$) fixed. Lower dots show the sites in absence of external forces, where $x_l = 0$ for all l . Upper dots sketch the positions after application of an external force f acting on site j . This yields $x_l = x_j$ for all $l < j$, implying a staircase form of the response matrix.

constrained modes capable of opposing elastic deformation (resembling a solid) [26, 27]. The resulting structure of \mathbf{W} then admits an orthogonal decomposition into free modes enabling fluid-like instantaneous response and constrained modes producing a delayed mechanical response, despite the absence of inertia. In particular, we demonstrate that the free modes exclusively govern the steady state response, while the constrained modes exclusively govern the relaxation after cessation of forcing. This allows for a clean (experimental) distinction between these modes. We exemplify these findings in a setup of a sheared fluid with viscoelastic components.

The paper is organized as follows. Sec. II is a preface, aimed to induce some intuition for the findings to follow. In Sec. III, we introduce the model, formulate the problem, and derive the formal solution. In Sec. IV, we cast the dynamics as an eigenvalue problem and obtain an exact diagonalization along with the corresponding eigenmodes. In Sec. V, we discuss the linear response of the system to external perturbations. In Sec. VI, we focus on the case of a rank-deficient interaction matrix, which enables an orthogonal decomposition of the state space into constrained and free modes and illustrate this structure through a physically motivated example in Sec. VII. Finally, Sec. VIII presents conclusions.

II. PREFACE: THE MASSLESS UNDAMPED CHAIN

Consider a chain of harmonically coupled particles with one end free and one end fixed, and the particles in the chain to be massless and frictionless. In this case, if a force acts on particle j , all particles i with $i < j$ will respond *in the same way* as particle j , as they are force free if relative distances are kept (see Fig. 1). In particular, the response of particle $i < j$ is independent of the properties or the length of the part of the chain in between i and j . As the response is reciprocal, this statement can be generalized: The response of an arbitrary particle i to a force acting on an arbitrary particle j is independent of the properties or the length of the part of the chain in between i and j . Inversion of the interaction matrix demonstrates similar properties for the static equilibrium correlations of the mentioned chain.

While a massless system may be hard to realize in practice, we demonstrate in this manuscript that a chain of overdamped Kelvin-Voigt units shows, among other things, the mentioned properties, which has various experimental ways of realization.

III. MODEL

We consider a one-dimensional chain of N interacting degrees of freedom (DoFs) with nearest-neighbor interactions. Each DoF $x_i(t)$ is coupled elastically with a harmonic spring of stiffness κ_i , and connected dissipatively with a dashpot of friction coefficient γ_i to its neighbor, $x_{i+1}(t)$ (see Fig. 2). Additionally, x_i is subject to a force f_i . The equation of motion for degree x_i is given by,

$$\gamma_i(\dot{x}_i - \dot{x}_{i+1}) + \gamma_{i-1}(\dot{x}_i - \dot{x}_{i-1}) + \kappa_i(x_i - x_{i+1}) + \kappa_{i-1}(x_i - x_{i-1}) = f_i; \quad \forall i = 1, \dots, N. \quad (1)$$

We consider a free boundary condition at one end, $x_0 = x_1$, and a fixed boundary condition at the other, $x_{N+1} = 0$. Thus, the system can be regarded as a collection of Kelvin-Voigt units [23–25]. The set of equations in Eq. (1) can be formulated compactly in terms of a state vector, $\mathbf{x} = \{x_1, x_2, \dots, x_N\}^T \in \mathbb{R}^N$, comprising the N DoFs,

$$\Gamma \dot{\mathbf{x}} + \mathbf{K} \mathbf{x} = \mathbf{f}, \quad (2)$$

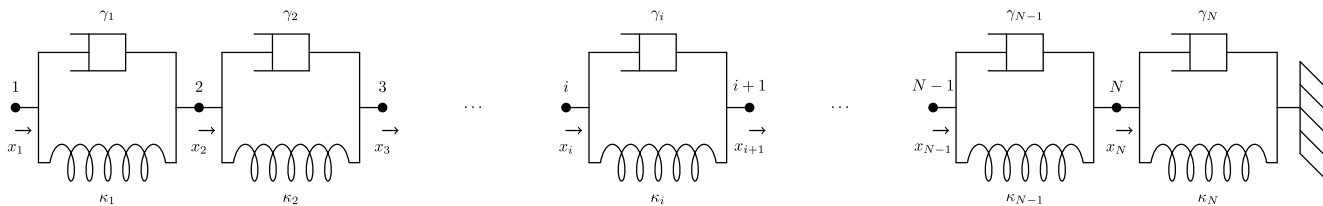


FIG. 2. **Schematic diagram of the model in Eq. (1)**, consisting of N interacting DoFs with nearest-neighbor interaction κ_i , and relative friction γ_i . The left end is free while the right end is fixed, $x_{N+1} = 0$. The model thus represents a chain of Kelvin-Voigt units [23–25].

where, the force $\mathbf{f} \in \mathbb{R}^N$, is given by, $\mathbf{f} = \{f_1, \dots, f_N\}^\top$. The matrices, $\Gamma, \mathbf{K} \in \mathbb{R}^{N \times N}$, encoding *friction* and *stiffness*, respectively, are tridiagonal, reflecting the nearest-neighbor interactions via dashpots and springs,

$$\Gamma_{ij} = (\gamma_i + \gamma_{i-1}) \delta_{ij} - \gamma_i \delta_{i+1,j} - \gamma_{i-1} \delta_{i-1,j}, \quad (3)$$

$$\mathbf{K}_{ij} = (\kappa_i + \kappa_{i-1}) \delta_{ij} - \kappa_i \delta_{i+1,j} - \kappa_{i-1} \delta_{i-1,j}. \quad (4)$$

We consider $\gamma_i > 0$, which makes Γ positive definite and ensures that the inverse, Γ^{-1} , exists. Moreover, we consider $\kappa_i \geq 0$, i.e., we allow zero values for κ_i , to be discussed in detail in Sec. VI. The formal solution of Eq. (2) for time t is given by,

$$\mathbf{x}(t) = e^{-\mathbf{W}(t-t_0)} \mathbf{x}(t_0) + \int_{t_0}^t ds e^{-\mathbf{W}(t-s)} \Gamma^{-1} \mathbf{f}(s). \quad (5)$$

$\mathbf{W} = \Gamma^{-1} \mathbf{K}$ is the *drift* matrix, and $\mathbf{x}(t_0)$, with $t_0 < t$, is the initial state. Thus, the time evolution is governed by the propagator $\exp(-\mathbf{W}t)$, requiring identification of the eigenmodes of \mathbf{W} . We turn to the problem of diagonalizing \mathbf{W} in the next section.

IV. EIGENMODES

The drift matrix, $\mathbf{W} = \Gamma^{-1} \mathbf{K}$, is non-symmetric, $\mathbf{W}^\top \neq \mathbf{W}$, since Γ and \mathbf{K} do not commute, $[\Gamma, \mathbf{K}] \neq 0$. Therefore, it is not *a priori* clear whether its eigenvectors form a well-behaved basis. To establish such a representation, one requires completeness together with orthogonality, which is determined by the choice of inner product. Equipping the space with the Γ -weighted inner product, $\langle \mathbf{a}, \mathbf{b} \rangle_\Gamma := \langle \mathbf{a} | \Gamma | \mathbf{b} \rangle$ [28], renders the operator \mathbf{W} self-adjoint, i.e., one may show,

$$\langle \mathbf{W} \mathbf{a}, \mathbf{b} \rangle_\Gamma = \langle \mathbf{a}, \mathbf{W} \mathbf{b} \rangle_\Gamma. \quad (6)$$

By virtue of the spectral theorem [29] for self-adjoint operators in finite-dimensional vector spaces, it then follows that \mathbf{W} is diagonalizable with real eigenvalues, and its eigenvectors can be chosen to form a complete orthonormal basis with respect to $\langle \cdot, \cdot \rangle_\Gamma$. Thus, dissipation Γ arises naturally as the suitable metric within the vector space \mathbb{R}^N .

Eq. (6) relies only on the positivity of Γ and the symmetry of \mathbf{K} , so that for any such case, \mathbf{W} has eigenvectors that form a complete orthonormal basis.

While the spectral theorem guarantees the existence of a complete orthonormal eigenbasis, it does not, as such, provide an explicit construction of the eigenmodes when Γ and \mathbf{K} do not commute. In heterogeneous systems, e.g., cases where γ_i or κ_i vary with i , this typically renders the analytical diagonalization of \mathbf{W} intractable. Nonetheless, in the case of Eq. (1), the tridiagonal structure of matrices, Γ, \mathbf{K} , in Eqs. (3), (4) enables analytical diagonalization of \mathbf{W} . To exploit this structure, we introduce the forward difference (discrete derivative) operator \mathbf{L} , given by,

$$\mathbf{L}_{ij} = \delta_{ij} - \delta_{i,j+1}; \quad (\mathbf{L} \mathbf{x})_i = x_i - x_{i+1}. \quad (7)$$

This operator maps site variables to bond variables (relative displacements), in which the dynamics simplifies considerably. Mathematically, \mathbf{L} allows to express Γ and \mathbf{K} as congruence transformations [30],

$$\Gamma = \mathbf{L}^\top \Lambda_\Gamma \mathbf{L}, \quad \mathbf{K} = \mathbf{L}^\top \Lambda_\mathbf{K} \mathbf{L}, \quad (8)$$

with, $\Lambda_\Gamma = \text{diag}\{\gamma_1, \gamma_2, \dots, \gamma_N\}$, and $\Lambda_K = \text{diag}\{\kappa_1, \kappa_2, \dots, \kappa_N\}$. Note that Eqs. (8) are not to be confused with diagonalization of Γ and K , as $L^\top \neq L^{-1}$. L however allows to diagonalize W , by use of the representations of Γ and K given in Eq. (8),

$$W = \Gamma^{-1}K = L^{-1}\Lambda_\Gamma^{-1}\Lambda_K L. \quad (9)$$

This is a similarity transform [31] that diagonalizes W to Λ ,

$$\Lambda := \Lambda_\Gamma^{-1}\Lambda_K = \text{diag}\left\{\frac{\kappa_1}{\gamma_1}, \frac{\kappa_2}{\gamma_2}, \dots, \frac{\kappa_N}{\gamma_N}\right\}. \quad (10)$$

We identify L^{-1} from Eq. (9) to consist of the eigenvectors of W as columns (see App. A). The eigenvectors $\{|n\rangle\}$ satisfy,

$$W|n\rangle = \lambda_n|n\rangle; \quad \lambda_n := \frac{\langle n|\Gamma W|n\rangle}{\langle n|\Gamma|n\rangle} = \frac{\langle n|K|n\rangle}{\langle n|\Gamma|n\rangle} = \frac{\kappa_n}{\gamma_n}. \quad (11)$$

The eigenvalues $\{\lambda_n\}$ in Eq. (10) correspond to relaxation rates of the associated eigenmodes.

Moreover, the eigenvectors are orthogonal with respect to the inner product,

$$\langle n|\Gamma|m\rangle = \gamma_n\delta_{nm}, \quad (12)$$

and form a complete set of basis,

$$\sum_n \frac{1}{\gamma_n} |n\rangle \langle n|\Gamma = \mathbf{1}. \quad (13)$$

In the eigenbasis, the displacement $|x\rangle$ can be expressed as,

$$|x\rangle = \sum_{n=1}^N y_n |n\rangle, \quad y_n := \frac{\langle n|\Gamma|x\rangle}{\langle n|\Gamma|n\rangle} = \frac{1}{\gamma_n} \langle n|\Gamma|x\rangle = x_n - x_{n+1}. \quad (14)$$

$\{y_n\}$ correspond to the eigenmode amplitudes or simply, eigenmodes, as projections onto the eigenvectors of W . Equation of motion in Eq. (1) decouples in the eigenbasis as eigenmode y_n evolves via,

$$\dot{y}_n + \lambda_n y_n = \frac{1}{\gamma_n} \langle n|\Gamma\Gamma^{-1}|f\rangle = \frac{1}{\gamma_n} \langle n|f\rangle; \quad (15)$$

we introduce the following notation for the transformed force,

$$F_n = \langle n|f\rangle = \sum_{i=1}^n f_i. \quad (16)$$

Thus, the force F_n for eigenmode n is a sum of forces f_i from 1 to n . Finally, we rewrite Eq. (15),

$$\gamma_n \dot{y}_n + \kappa_n y_n = F_n, \quad (17)$$

with the solution,

$$y_n(t) = e^{-\frac{\kappa_n}{\gamma_n}(t-t_0)} y_n(t_0) + \int_{t_0}^t dt' e^{-\frac{\kappa_n}{\gamma_n}(t-t')} \frac{F_n(t')}{\gamma_n}. \quad (18)$$

Eq. (18) will be used in finding the systems susceptibility in the coming section.

Using the definition in Eq. (14), one constructs $\mathbf{y} = (y_1, \dots, y_N)^\top$, and finds from Eq. (7),

$$\mathbf{y} = \mathbf{L}\mathbf{x}; \quad y_i = x_i - x_{i+1}. \quad (19)$$

As anticipated, the eigenmodes correspond to the bonds, i.e., to the relative displacements between two neighboring DoFs (see Fig. 3), whose dynamics is thus decoupled. The displacements \mathbf{x} are found from the eigenmodes \mathbf{y} by inversion of Eq. (19),

$$\mathbf{x} = \mathbf{L}^{-1}\mathbf{y}; \quad x_i = \sum_{j=i}^N y_j. \quad (20)$$

Hence, \mathbf{L}^{-1} acts as a cumulative sum (discrete integration) operator with elements,

$$(\mathbf{L}^{-1})_{ij} = \begin{cases} 1, & i \leq j, \\ 0, & i > j; \end{cases} \quad (\mathbf{L}^{-1}\mathbf{x})_i = \sum_{j=i}^N x_j. \quad (21)$$

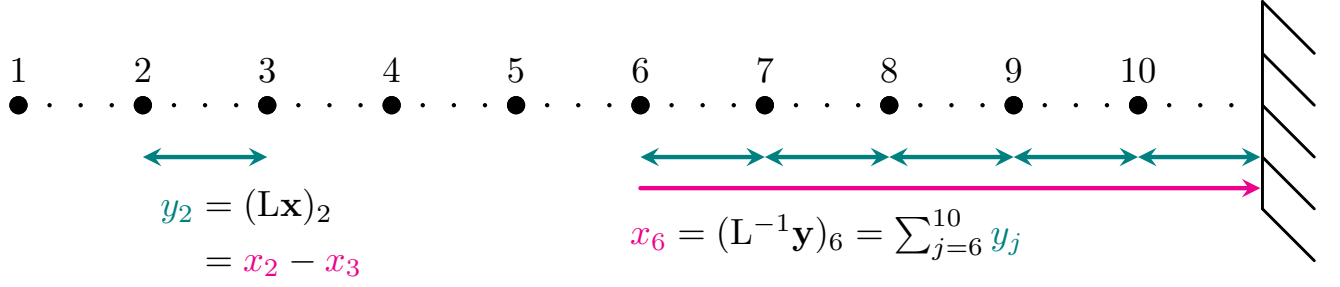


FIG. 3. **Schematic for eigenmodes**, exemplarily for $N = 10$. Left part of sketch demonstrates the eigenmode $i = 2$ via application of L , see Eq. (19). Right part of sketch illustrates action of L^{-1} to obtain x_6 from eigenmodes, see Eq. (20).

V. RESPONSE: “X-RAY VISION” AND INFINITE RANGE

We aim to find the linear response of $\mathbf{x}(t)$ to the application of a time-dependent force vector $\mathbf{f}(t)$,

$$\mathbf{x}(t) = \int_{-\infty}^t dt' \chi(t-t') \mathbf{f}(t'), \quad (22)$$

with the susceptibility $\chi(t) \in \mathbb{R}^{N \times N}$, formally defined as,

$$\chi_{ij}(t-t') = \left. \frac{\delta x_i(t)}{\delta f_j(t')} \right|_{\mathbf{f}=\mathbf{0}}. \quad (23)$$

$\chi_{ij}(t)$ thus quantifies the response at site i due to a force applied at site j . $\chi(t)$ can be read off from Eq. (5), letting $t_0 \rightarrow -\infty$,

$$\chi(t) = \Theta(t) \exp(-Wt) \Gamma^{-1}. \quad (24)$$

$\Theta(t)$ is the Heaviside step function owing to causality. We may further express $\chi(t)$ in the diagonal representation,

$$\chi(t) = \Theta(t) L^{-1} e^{-\Lambda t} \Lambda_{\Gamma}^{-1} (L^{-1})^{\top}, \text{ i.e., } \chi_{ij}(t) = \Theta(t) L_{il}^{-1} \left(\frac{1}{\gamma_l} e^{-\frac{\kappa_l}{\gamma_l} t} \right) L_{jl}^{-1}. \quad (25)$$

We used, $(L^{-1})_{lj}^{\top} = L_{jl}^{-1}$, and adopted Einstein summation convention where summation over repeated indices is implied. Plugging L^{-1} from Eq. (21) in Eq. (25), $\chi_{ij}(t)$ can be expressed as,

$$\chi_{ij}(t) = \Theta(t) \sum_{l=\max\{i,j\}}^N \frac{1}{\gamma_l} e^{-\frac{\kappa_l}{\gamma_l} t}. \quad (26)$$

This expression has an intriguing and transparent origin (see Fig. 4):

1. A force f_j applied at site j yields a force F_l from Eq. (16),

$$F_l = f_j \Theta(l-j) = \begin{cases} 0, & l < j; \\ f_j, & l \geq j. \end{cases} \quad (27)$$

In other words, the force f_j only affects eigenmodes with $l \geq j$.

2. The displacement (response) at site i is obtained by summing over eigenmodes l with $l \geq i$, see Eq. (20).
3. As a result of these two observations, the response $\chi_{ij}(t)$ involves only those eigenmodes that lie in the overlap of these two regions, namely $l \geq \max\{i, j\}$, as indicated in Eq. (26).

The susceptibility thus naturally reflects the cumulative nature of both force transmission and displacement reconstruction, leading to the compact structure in Eq. (26). The susceptibility in Eq. (26) has the following physical properties that are worth noting:

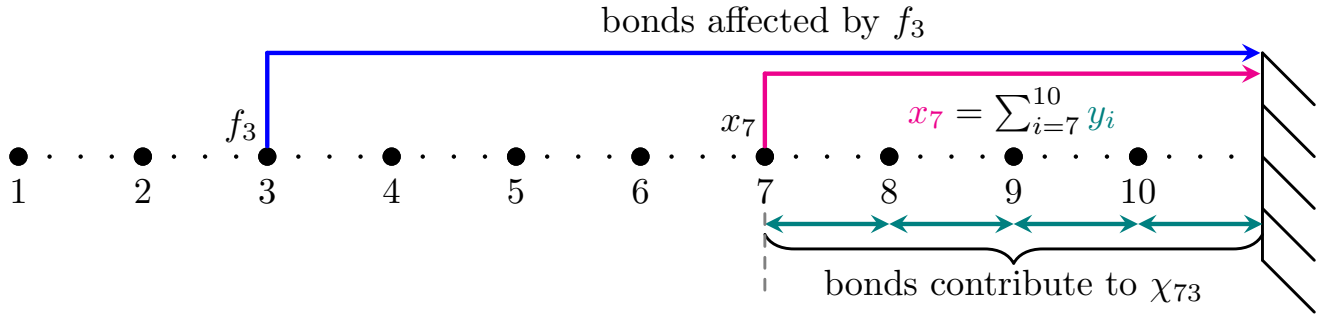


FIG. 4. **Schematic for the susceptibility** χ_{ij} in Eq. (26), quantifying the response at site i to a force at site j , exemplarily for $N = 10$. A force acting on $j = 3$ yields, via Eq. (16), a finite force F_l for $l \geq 3$, so that these bonds show a response to the force. On the other hand, the response at site $i = 7$ is found from the bonds with $l \geq 7$, see Eq. (20). Hence, the susceptibility $\chi_{73} = \chi_{37}$ has contributions from bonds $l \geq \max\{7, 3\}$, i.e., $l \geq 7$.

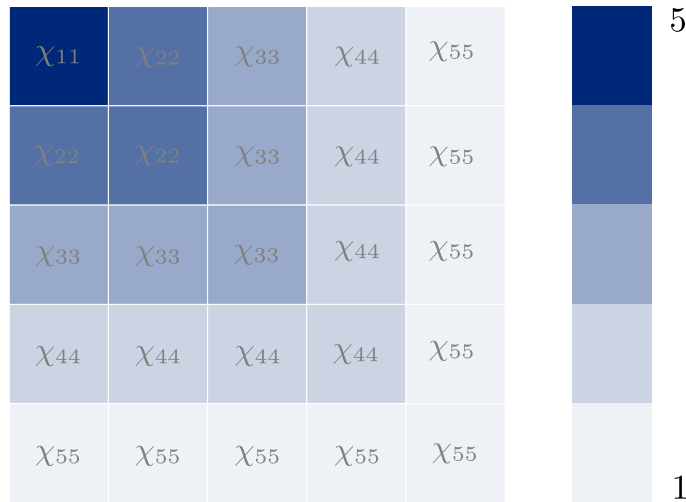


FIG. 5. **Susceptibility matrix**, exemplarily for $N = 5$. The color-code gives the number of bonds contributing to the respective element χ_{ij} according to Eq. (26). Any element χ_{ij} equals a diagonal entry, i.e., $\chi_{ij} = \chi_{ji} = \chi_u$ with $l = \max\{i, j\}$.

1. “X-ray vision”: The response of site i to a force acting on site j is *independent* of the properties of sites with $l < \max\{i, j\}$. It is especially independent of the properties of the sites that lie in between i and j , i.e., the response *sees through* the sites in between i and j . As an extreme example: The response of site N to a force acting on site 1 depends only on κ_N and γ_N . As the susceptibility is symmetric, this also applies to the response of site 1 to a force acting on site N .
2. Infinite range: The response is of infinite range as it does not depend on the number of sites located between i and j .
3. Any off diagonal entry equals a diagonal one, i.e., $\chi_{ij}(t) = \chi_u(t)$ with $l = \max\{i, j\}$. As a consequence, the susceptibility matrix may at most contain N different entries (see Fig. 5).
4. The response χ_{ii} does not depend on the order of the bonds with $l \geq i$. As an extreme example, χ_{11} , i.e., the response of site 1 to a force acting on site 1, does not depend on the order of the bonds in the chain.

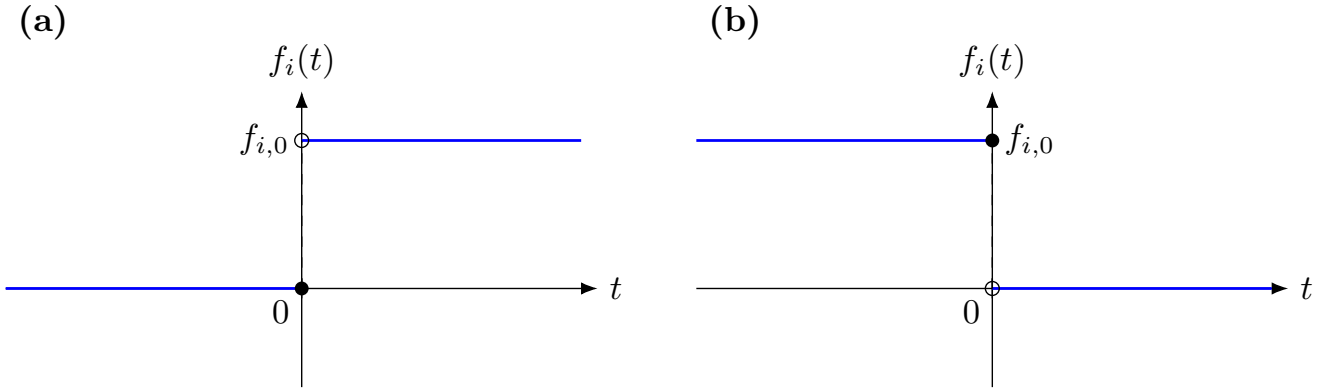


FIG. 6. **Protocols designed to specifically probe the free and constrained modes.** (a) “Steady driving” as depicted in Eq. (31) where force acts only at $t > 0$, revealing the free modes. (b) “Relaxation” as depicted in Eq. (34), where force only acts at $t \leq 0$, unveiling the constrained modes for $t > 0$.

VI. RANK-DEFICIENT INTERACTION: TWO SETS OF DISTINCT MODES

A. Constrained and free modes

An interesting example concerns the case of a rank-deficient interaction matrix, as it leads to distinct types of response. We may partition the set of bonds, $\mathcal{B} = \{1, \dots, N\}$, into two subsets: constrained bonds, $i \in \mathcal{B}_\kappa$, correspond to nonzero stiffness coefficients, $\kappa_i > 0$, while free bonds, $i \in \mathcal{B}_0$, correspond to $\kappa_i = 0$, with $\mathcal{B}_0 = \mathcal{B} \setminus \mathcal{B}_\kappa$,

$$\kappa_i = \begin{cases} > 0, & i \in \mathcal{B}_\kappa, \\ 0, & i \in \mathcal{B}_0. \end{cases} \quad (28)$$

The presence of free bonds renders the stiffness matrix \mathbf{K} rank-deficient and partitions the chain into disconnected segments. Each such segment supports a mode responding to rigid translation without restoring force. Consequently, the spectrum of the drift operator \mathbf{W} contains zero eigenvalues (cf. Eq. (10)), and the state space decomposes into two physically distinct subspaces: the null space $\text{null}(\mathbf{W})$, spanned by the modes with $\kappa_i = 0$, and a complementary subspace, the image space $\text{im}(\mathbf{W})$, spanned by the modes with finite κ_i ,

$$\mathbb{R}^N = \text{null}(\mathbf{W}) \oplus \text{im}(\mathbf{W}). \quad (29)$$

This distinction is directly reflected in the dynamics. From Eqs. (15), modes associated with nonzero eigenvalues relax exponentially in time due to restoring forces ($\kappa_i \neq 0$), whereas the free modes, in absence of external forces, do not evolve. The dynamics therefore separates naturally into relaxing (constrained) and steady (unconstrained) components.

The linear response of the system in Eq. (26) can in this case be written as,

$$\chi_{ij}(t) = \Theta(t) \left(\sum_{\substack{l \in \mathcal{B}_0 \\ l \geq \max\{i,j\}}} \frac{1}{\gamma_l} + \sum_{\substack{l \in \mathcal{B}_\kappa \\ l \geq \max\{i,j\}}} \frac{1}{\gamma_l} e^{-\frac{\kappa_l}{\gamma_l} t} \right). \quad (30)$$

The susceptibility thus naturally decomposes into two contributions associated with distinct dynamical subspaces. Free modes correspond to \mathcal{B}_0 (equivalently, $\text{null}(\mathbf{W})$) as they respond instantaneously to external perturbations, producing a time-independent purely viscous contribution. In contrast, constrained modes are associated with \mathcal{B}_κ (equivalently, $\text{im}(\mathbf{W})$), and they exhibit exponentially decaying responses, reflecting their elastic component.

In the two next subsections, we will elucidate driving protocols that exclusively probe one of the two subspaces.

B. Steady driving: Probing the free modes

We start with the case of a steady driving, i.e.,

$$f_i(t) = \begin{cases} 0 & t \leq 0, \\ f_{i,0} & t > 0. \end{cases} \quad (31)$$

In this case, the solution for $x_i(t)$ from Eq. (5) is given by,

$$x_i(t) = \Theta(t) \left(\sum_{\substack{l \in \mathcal{B}_0 \\ l \geq i}} \frac{F_{l,0} t}{\gamma_l} + \sum_{\substack{l \in \mathcal{B}_\kappa \\ l \geq i}} \frac{F_{l,0}}{\kappa_l} (1 - e^{-\frac{\kappa_l}{\gamma_l} t}) \right); \quad (32)$$

with $F_{l,0} = \sum_{j=1}^l f_{j,0}$, as in Eq. (16). The steady state is reached when all modes with finite κ have relaxed, and the steady state velocity \dot{x}_i is completely determined by the free modes,

$$\lim_{t \rightarrow \infty} \dot{x}_i(t) = \sum_{\substack{l \in \mathcal{B}_0 \\ l \geq i}} \frac{F_{l,0}}{\gamma_l}. \quad (33)$$

C. Relaxation: Probing the constrained modes

We consider in this section the opposite protocol scenario to the above, namely,

$$f_i(t) = \begin{cases} f_{i,0} & t \leq 0, \\ 0 & t > 0. \end{cases} \quad (34)$$

The force applied during negative times gives rise to an initial condition $\mathbf{x}(t=0)$. The solution for $t > 0$ is then found from Eq. (5), by setting $\mathbf{f} = \mathbf{0}$,

$$\mathbf{x}(t) = e^{-\mathbf{W}t} \mathbf{x}(0), \quad (35)$$

$$\dot{\mathbf{x}}(t) = -\mathbf{W}e^{-\mathbf{W}t} \mathbf{x}(0). \quad (36)$$

For the eigenmodes,

$$\mathbf{y}(t) = e^{-\Lambda t} \mathbf{y}(0), \quad (37)$$

$$\dot{\mathbf{y}}(t) = -\Lambda e^{-\Lambda t} \mathbf{y}(0). \quad (38)$$

with the diagonal matrix Λ given in Eq. (10). Eq. (38) shows that only the non-zero eigenvalues contribute to motion for positive times,

$$\dot{y}_i(t > 0) = \begin{cases} 0, & \forall i \in \mathcal{B}_0; \\ -\frac{F_{i,0}}{\gamma_i} e^{-\frac{\kappa_i}{\gamma_i} t}, & \forall i \in \mathcal{B}_\kappa. \end{cases} \quad (39)$$

As before, $F_{i,0} = \sum_{j=1}^i f_{j,0}$. The negative sign signifies that the relaxation motion (recoil) is in the direction opposite to driving $f_{i,0}$ [32–35]. For the DoF x_i , we finally have for $t > 0$,

$$\dot{x}_i(t) = \sum_{\substack{l \geq i \\ l \in \mathcal{B}_\kappa}} \dot{y}_l(t) = - \sum_{\substack{l \geq i \\ l \in \mathcal{B}_\kappa}} \frac{F_{l,0}}{\gamma_l} e^{-\frac{\kappa_l}{\gamma_l} t}. \quad (40)$$

This shows that the relaxation dynamics is solely governed by the constrained modes.

In summary, when the force that has been acting for a long time is switched off, the motion of all sites instantaneously changes from being completely governed by the free modes to being completely governed by the constrained modes. Such protocol thus enables detection of the two sets of modes individually.

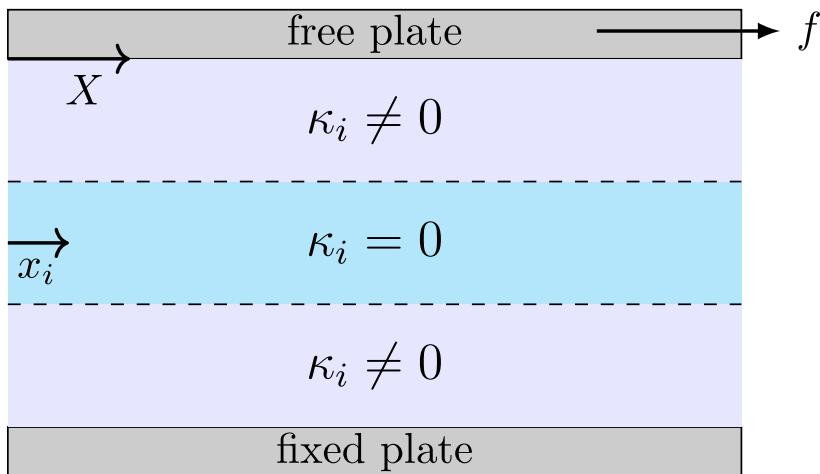


FIG. 7. **Viscoelastic fluid confined in-between two parallel plates.** The lower plate is fixed, while the upper plate is subject to a force f . The fluid is divided into three regions: viscoelastic regions (purple) located near both plates, characterized by $\kappa_i \neq 0$, and a purely viscous region (sky blue) sandwiched between them, where $\kappa_i = 0$. When the upper plate is driven, the layers of the fluid are sheared. The lateral displacement of layer i is denoted by x_i , while the displacement of the upper plate is denoted by X .

VII. EXAMPLE: VISCOELASTIC FLUID IN CONFINEMENT

We aim to illustrate the above findings in an example system of a confined fluid. Consider a simple fluid confined between two parallel plates. The lower plate is kept fixed, while the upper plate is free to move laterally, and subject to a time dependent force $f(t)$. The coordinates x_i correspond to lateral displacements of the corresponding fluid layer at height indexed by i , with $x_1 \equiv X$, the position of the upper plate. The vicinities of the plates possess finite restoring forces, e.g., corresponding to polymer brushes attached to the surfaces of the plates. This is mimicked by finite values of κ_i close to the two plates. The simple fluid in between the plates is modelled by $\kappa_i = 0$ (see Fig. 7). The following statements hold true for any positive values of γ_i and any non-negative κ_i .

- Under a time independent force f , the steady state velocity of the upper plate only depends on the bulk region, i.e., only on the free modes with $\kappa_i = 0$,

$$\lim_{t \rightarrow \infty} \dot{X}(t) = f \sum_{l \in \mathcal{B}_0} \frac{1}{\gamma_l}. \quad (41)$$

- After switching off the force, the recoil motion of the upper plate is solely determined by the constrained modes with $\kappa_i \neq 0$,

$$\dot{X}(t) = -f \sum_{l \in \mathcal{B}_\kappa} \frac{1}{\gamma_l} e^{-\frac{\kappa_l}{\gamma_l} t}. \quad (42)$$

- The above statements, i.e., Eqs. (41) and (42), do not depend on the order of the segments. For example, exchanging the positions of the three regions in Fig. 7 has no effect on the response of X .
- The response of any layer to the force f applied to the upper plate is independent of the material above the respective layer. For example, the response of the bulk fluid in the center is independent of the polymer layer attached to the upper plate.

This example provides a direct physical realization of the decomposition into free and constrained modes: steady driving probes the free (unconstrained) subspace, whereas transient relaxation reveals the constrained subspace.

VIII. CONCLUSION

We developed an exact analytical framework for a class of heterogeneous overdamped chains with harmonic interactions and momentum-conserving dissipation. Despite the non-symmetric nature of the drift operator $W = \Gamma^{-1}K$, we

demonstrate that its structure admits an exact diagonalization through a forward-difference transformation, mapping the dynamics from node to bond variables. This holds in the presence of heterogeneity in terms of interactions or damping.

A central result is the emergence of a staircase structure in the linear response function as illustrated in Figs. 4, 5. The susceptibility χ_{ij} depends only on modes l with $l \geq \max\{i, j\}$, leading to the striking consequence that the response between two sites is independent of the properties of the system in between them. This ‘‘X-ray vision’’ property implies an effectively infinite-range response and a highly constrained structure of the susceptibility matrix, with at most N distinct entries.

We further showed that when the interaction matrix is rank-deficient, the dynamics naturally decomposes into two physically distinct subspaces. Free modes, associated with zero eigenvalues, produce an instantaneous, purely viscous response and the steady-state behavior under sustained driving is exclusively governed by these modes. In contrast, the transient relaxation dynamics after removal of forcing, is exclusively governed by the constrained modes, associated with finite eigenvalues. This separation provides a way of individual probing of the two types of modes via choice of protocol.

The mentioned properties were illustrated in the example of a fluid under shear. Beyond the simple-shear geometry considered here, the present framework can be extended to a broader class of flow configurations, including other shear geometries such as Taylor–Couette flow [36, 37]. More generally, the model also provides a natural description of the response of rotating objects embedded in viscoelastic fluids, where the perturbation is generated not by an external force but by an applied torque acting again at a *free end*. This opens a route toward analytically characterizing torsional microrheology and torque-driven viscoelastic response within the same unified framework [38].

Our results highlight how momentum-conserving dissipation fundamentally alters the structure of overdamped dynamics. Rather than destroying analytical tractability, the combination of relative friction and nearest-neighbor interactions imposes a structure that enables an exact solution, even in heterogeneous systems. This stands in contrast to conventional overdamped models with local friction, where heterogeneity typically precludes closed-form analysis.

The framework developed here opens several directions for future research. A natural extension is to incorporate stochastic forces and investigate fluctuation properties, in particular in cases where stochastic forces do not obey equilibrium properties. Another promising direction is the study of time-dependent or disordered network topologies, where bonds may dynamically appear or disappear, potentially leading to non-trivial aging or memory effects. Non-reciprocal bonds are also of interest. Extending the analysis to higher-dimensional networks or more complex geometries could reveal how the ‘‘X-ray’’ response generalizes beyond one dimension. Finally, introducing nonlinear interactions or coupling to external flows may provide a route to understanding emergent viscoelastic behavior in driven soft-matter systems and complex fluids.

ACKNOWLEDGMENTS

This project was funded by the Deutsche Forschungsgemeinschaft (DFG), Grant No. SFB 1432–Project ID 425217212, Project C05. We thank Clemens Bechinger and Niloyendu Roy for a critical reading of the manuscript and for useful comments.

Appendix A: Explicit Forms

The equations of motion for N interacting DoFs, where x_i corresponds to the deviation of i^{th} DoF from its equilibrium (mean) position, are given by the following set of coupled linear differential equations,

$$\begin{aligned} m_1 \ddot{x}_1 &= -\gamma_1(\dot{x}_1 - \dot{x}_2) - \kappa_1(x_1 - x_2) + f_1, \\ m_i \ddot{x}_i &= -\gamma_i(\dot{x}_i - \dot{x}_{i+1}) - \gamma_{i-1}(\dot{x}_i - \dot{x}_{i-1}) - \kappa_i(x_i - x_{i+1}) - \kappa_{i-1}(x_i - x_{i-1}) + f_i, \quad \forall i = 2, 3, \dots, N-1; \\ m_N \ddot{x}_N &= -\gamma_N \dot{x}_N - \gamma_{N-1}(\dot{x}_N - \dot{x}_{N-1}) - \kappa_N x_N - \kappa_{N-1}(x_N - x_{N-1}) + f_N. \end{aligned} \quad (\text{A1})$$

This set of equations are expressed compactly in Eq. (1) of the main text, after taking the overdamped limit, i.e., $m \rightarrow 0$.

The friction matrix Γ is explicitly given below,

$$\Gamma = \begin{pmatrix} \gamma_1 & -\gamma_1 & 0 & \cdots & 0 & 0 \\ -\gamma_1 & \gamma_1 + \gamma_2 & -\gamma_2 & \ddots & & \vdots \\ 0 & -\gamma_2 & \gamma_2 + \gamma_3 & \ddots & \ddots & 0 \\ \vdots & \ddots & \ddots & \ddots & -\gamma_{N-2} & 0 \\ 0 & & \ddots & -\gamma_{N-2} & \gamma_{N-2} + \gamma_{N-1} & -\gamma_{N-1} \\ 0 & \cdots & 0 & 0 & -\gamma_{N-1} & \gamma_{N-1} + \gamma_N \end{pmatrix} \quad (\text{A2})$$

The stiffness matrix K is explicitly given below,

$$K = \begin{pmatrix} \kappa_1 & -\kappa_1 & 0 & \cdots & 0 & 0 \\ -\kappa_1 & \kappa_1 + \kappa_2 & -\kappa_2 & \ddots & & \vdots \\ 0 & -\kappa_2 & \kappa_2 + \kappa_3 & \ddots & \ddots & 0 \\ \vdots & \ddots & \ddots & \ddots & -\kappa_{N-2} & 0 \\ 0 & & \ddots & -\kappa_{N-2} & \kappa_{N-2} + \kappa_{N-1} & -\kappa_{N-1} \\ 0 & \cdots & 0 & 0 & -\kappa_{N-1} & \kappa_{N-1} + \kappa_N \end{pmatrix} \quad (\text{A3})$$

The forward difference matrix L , and its inverse L^{-1} , representing cumulative sum, are given below,

$$L = \begin{pmatrix} 1 & -1 & 0 & 0 & \cdots & 0 \\ 0 & 1 & -1 & 0 & \cdots & 0 \\ 0 & 0 & 1 & -1 & \cdots & 0 \\ \vdots & \vdots & \ddots & \ddots & \ddots & \vdots \\ 0 & 0 & \cdots & 0 & 1 & -1 \\ 0 & 0 & \cdots & 0 & 0 & 1 \end{pmatrix}; \quad L^{-1} = \begin{pmatrix} 1 & 1 & 1 & \cdots & 1 \\ 0 & 1 & 1 & \cdots & 1 \\ 0 & 0 & 1 & \cdots & 1 \\ \vdots & \vdots & \vdots & \ddots & 1 \\ 0 & 0 & 0 & \cdots & 1 \end{pmatrix} \quad (\text{A4})$$

-
- [1] M. Bennett, M. F. Schatz, H. Rockwood, and K. Wiesenfeld, *Proceedings of the Royal Society A: Mathematical, Physical and Engineering Sciences* **458**, 563 (2002).
- [2] H. Goldstein, C. Poole, and J. Safko, *Classical Mechanics*, 3rd ed. (Addison Wesley, Boston, 2002).
- [3] A. Einstein, *Annalen der Physik* **327**, 180–190 (1907).
- [4] M. Born and T. von Kármán, *Physikalische Zeitschrift* **13**, 297 (1912).
- [5] P. Debye, *Annalen der Physik* **344**, 789 (1912).
- [6] C. Kittel, *Introduction to Solid State Physics* (Wiley, 2004).
- [7] J. Rouse, Prince E., *The Journal of Chemical Physics* **21**, 1272 (1953).
- [8] A. Caldeira and A. Leggett, *Physica A: Statistical Mechanics and its Applications* **121**, 587–616 (1983).
- [9] M. Doi and S. F. Edwards, *The Theory of Polymer Dynamics*, Vol. 73 (Oxford University Press, 1988).
- [10] E. Rolls, Y. Togashi, and R. Erban, *Multiscale Modeling & Simulation* **15**, 1672–1693 (2017).
- [11] J.-H. Hung, J. H. Mangalana, and D. S. Simmons, *Macromolecules* **51**, 2887–2898 (2018).
- [12] X. Tian, Y. Chen, X. Xu, W.-S. Xu, and J. Chen, *The Journal of Chemical Physics* **158**, 204904 (2023).
- [13] B. S. Khatri and T. C. B. McLeish, *Macromolecules* **40**, 6770–6777 (2007).
- [14] R. R. Cheng, A. T. Hawk, and D. E. Makarov, *The Journal of Chemical Physics* **138**, 074112 (2013).
- [15] R. Kailasham, R. Chakrabarti, and J. R. Prakash, *Journal of Rheology* **65**, 903 (2021).
- [16] B. H. Zimm, *The Journal of Chemical Physics* **24**, 269 (1956).
- [17] P. J. Hoogerbrugge and J. M. V. A. Koelman, *Europhysics Letters* **19**, 155 (1992).
- [18] P. Español and P. Warren, *Europhysics Letters* **30**, 191 (1995).
- [19] P. Español, *Europhysics Letters* **40**, 631 (1997).
- [20] J. B. Avalos and A. D. Mackie, *Europhysics Letters* **40**, 141 (1997).
- [21] W. Jiang, J. Huang, Y. Wang, and M. Laradji, *The Journal of Chemical Physics* **126**, 044901 (2007).
- [22] D. Das, R. Vink, and M. Krüger, *Journal of Physics: Condensed Matter* **36**, 215707 (2024).
- [23] G. Shao-hua, *Applied Mathematics and Mechanics (English Edition)* **25**, 792 (2004).
- [24] A. Serra-Aguila, J. M. Puigoriol-Forcada, G. Reyes, and J. Menacho, *Acta Mechanica Sinica* **35**, 1191 (2019).
- [25] M. Trcala, P. Suchomelová, M. Bošanský, F. Hokeš, and I. Němec, *Mechanics of Time-Dependent Materials* **28**, 1639 (2024).

- [26] N. Phan-Thien, N. Mai-Duy, B. Khoo, and D. Duong-Hong, *Applied Mathematical Modelling* **40**, 6359–6375 (2016).
- [27] S. Tong, R. Sknepnek, and A. Košmrlj, *Phys. Rev. Res.* **5**, 013143 (2023).
- [28] In this section, we introduce the Dirac (bra-ket) notation for the ease of analysis: $|a\rangle \equiv \mathbf{a}$, $\langle a| \equiv \mathbf{a}^\top$.
- [29] S. Axler, *Linear Algebra Done Right* (Springer, 2024).
- [30] E. W. Weisstein, Congruence transformation, <https://mathworld.wolfram.com/CongruenceTransformation.html>, from MathWorld—A Wolfram Resource.
- [31] G. B. Arfken, H. J. Weber, and F. E. Harris, *Mathematical Methods for Physicists: A Comprehensive Guide* (Academic press, 2011).
- [32] F. Ginot, J. Caspers, L. F. Reinalter, K. Krishna Kumar, M. Krüger, and C. Bechinger, *New Journal of Physics* **24**, 123013 (2022).
- [33] J. Caspers, N. Ditz, K. Krishna Kumar, F. Ginot, C. Bechinger, M. Fuchs, and M. Krüger, *The Journal of Chemical Physics* **158**, 024901 (2023).
- [34] X. Cao, D. Das, N. Windbacher, F. Ginot, M. Krüger, and C. Bechinger, *Nature Physics* **19**, 1904 (2023).
- [35] S. S. Vaidya, L. Muruga, J. Caspers, M. Krüger, and C. Bechinger, *Phys. Rev. Res.* **7**, 033084 (2025).
- [36] G. I. Taylor, *Philosophical Transactions of the Royal Society of London, Series A: Containing Papers of a Mathematical or Physical Character* **223**, 289 (1923).
- [37] L. D. Landau and E. M. Lifshitz, *Fluid Mechanics: Volume 6*, 2nd ed. (Elsevier, 1987).
- [38] N. Roy, R. Saha, D. Das, C. Bechinger, and M. Krüger, Geometry-induced proliferation of memory effects in viscoelastic fluids (2026), in preparation.